Preconditioned Euler and Navier-Stokes Calculations on Unstructured Meshes

P. Moinier M.B. Giles
Oxford University Computing Laboratory
Numerical Analysis Group

1 Introduction

Multigrid techniques for unstructured meshes have proven to be very successful for both 2D and 3D inviscid problems, and recent advances concerning unstructured mesh generation, flow solvers and parallel computing techniques have made the predictions of these flows for complex geometries a rapid and robust procedure [3, 8, 11]. However, for an accurate aerodynamic analysis, viscous effects must be considered and to capture these, turbulence and transition modelling are required. The highly stretched computational cells, that are needed to efficiently resolve a high Reynolds number boundary layer limit the effectiveness of multigrid procedures which can not eliminate all the error modes which can exist in the solution. To overcome this drawback, different methods have been proposed. One is a semi-coarsening multigrid strategy, in which the mesh is not coarsened in every direction simultaneously [10], while others are based on the use of a preconditioner [1] which has the effect of moving the eigenvalues away from the origin of the Fourier complex plan providing, within an optimised Runge-Kutta update, a very good damping of the high-frequency error modes.
Recently, Pierce and Giles [12] have analysed different combinations of preconditioner and multigrid method for both inviscid and viscous flow applications on structured grids. It has turned out that for turbulent Navier-Stokes calculations, a block-Jacobi preconditioner and a J-coarsened multigrid method provide an effective damping of all modes inside the boundary layer. The preconditioner damps all the convective modes, while the multigrid strategy, in which the grids are coarsened only along the normal to the boundary layer, ensures that all acoustic modes disappear. Thus, they have demonstrated that considerable speed-up can be achieved when using stretched structured meshes.

The present work follows this idea, but uses an unstructured grid approach. The same preconditioner has been implemented in a multigrid solver which has proven to be highly successful for inviscid meshes [4, 2], and has been modified to treat the highly stretched grids required for high Reynolds number flows [5] so that the equivalent of a J-coarsening strategy is employed. In the following sections we describe how the local preconditioner is constructed, how the boundary conditions are treated, and exemplify the resulting method through 2D and 3D test cases.

2 Scheme Description

The pre-conditioned semi-discrete equation appears as

$$P^{-1}\frac{dQ}{dt} + R(Q) = 0, \tag{2.1}$$

where Q [1] denotes the set of conservative variables, $R(Q)$ the residual vector of the spatial discretisation and P^{-1} the local preconditioner. Since the spatial discretisation as the multigrid method are not the subject of this paper, the interested reader is referred to [5]. The block-Jacobi preconditioner is based on a local linearisation of the 3D Navier-Stokes equations, in a first order upwind discretisation and built by extracting the terms corresponding to the central node. As the flux can be split into inviscid and viscous parts, the matrix preconditioner has contributions coming from both.

2.1 The Inviscid Contribution

Using a finite volume approach, the integration of the inviscid terms over some control volume Ω gives, after the application of the divergence theorem,

$$R_i^I = \frac{1}{V_i} \oint_{\partial\Omega} \mathcal{F}^I(\mathbf{n}, \mathcal{Q}) dS, \tag{2.2}$$

where V_i is the measure of the control volume associated with index i, and $\mathcal{F}^I(\mathbf{n}, \mathcal{Q})$ is the inviscid flux in the direction of the unit vector $\mathbf{n}$. As explained in [5], the discrete approximation to equation (2.2) is

$$R_i^I = \frac{1}{V_i} \left(\sum_{j \in E_i} F_{ij}^I \triangle s_{ij} + \sum_{k \in B_i} F_{ik}^{I_b} \triangle s_{ik}^b \right), \quad \forall i \tag{2.3}$$

where F_{ij}^I is the numerical inviscid flux in the direction $\mathbf{n}_{ij}$ associated with an edge (i, j), and F^{I_b} is the one associated with a boundary face. E_i is the set of all nodes connected to node i via an edge, B_i the set of all boundary edges (2D) or faces (3D) connected to it, $\triangle s_{ij}$ and $\triangle s_{ik}^b$ a distance (2D) or area (3D) associated with the edge considered. The fluxes include the average of the flux at mid-edge plus some artificial dissipation which is a blend of second and fourth differences.
Following the same approach used successfully on structured grids [13], the preconditioner is based on a first order discretisation even though a high-order method with limiters is used to define R_i^I. Using first order characteristic smoothing, and a local linearisation about a uniform flow, the flux F_{ij}^I in (2.3) becomes

$$F_{ij}^I \approx \frac{1}{2} \left(A_{ij}(Q_i + Q_j) - |A_{ij}|(Q_j - Q_i) \right),$$

where $A_{ij} \equiv \partial F_{ij}^I / \partial Q$. Now $\sum_{j \in E_i} A_{ij} Q_i \triangle s_{ij} = 0$ since a flux integral of a uniform flow vector over a closed surface is zero. Hence, retaining only those terms affecting the central node, one gets the preconditioner

$$\left(P_i^I\right)^{-1} = \frac{1}{2V_i} \left(\sum_{j \in E_i} |A_{ij}| \triangle s_{ij} + \sum_{k \in B_i} |A_{ik}| \triangle s_{ik}^b \right). \tag{2.4}$$

2.2 The Viscous Contribution

The integration of the viscous terms follows the usual rule over each volume, equation (2.2), giving a consistent finite volume treatment of the inviscid and viscous fluxes. Consequently,

[1] In this paper Roman letters are used to denote discrete quantities, whereas calligraphic letters are used to denote analytic functions and variables. Bold quantities are vectors in Cartesian coordinates.

the viscous residual may be written

$$R_i^V = \frac{1}{V_i} \oint_{\partial\Omega} \mathcal{F}^V(\mathbf{n}, \mathcal{Q}, \nabla\mathcal{Q}) dS. \tag{2.5}$$

Following a linearising procedure, equation (2.5) is approximated using the same pre-computed edge weights as mentioned previously, but only for an interior grid point since there is no viscous contribution for a node which lies on a adiabatic solid wall at which the velocity is set to zero. Thus,

$$R_i^V = \frac{1}{V_i} \sum_{j \in E_i} F_{ij}^V \triangle s_{ij}, \quad \forall i \tag{2.6}$$

where F_{ij}^V is the numerical viscous flux in the direction $\mathbf{n}_{ij}$ associated with the edge (i, j). For convenience, to construct the viscous contribution of the matrix preconditioner the following approximations are made:

- All cross derivatives are neglected.
- $\nabla\mathcal{Q}$ is approximated by $\frac{\partial\mathcal{Q}}{\partial l}\mathbf{l}$, where $\mathbf{l}$ is a unit vector for the edge pointing from node i to node j and $\frac{\partial\mathcal{Q}}{\partial l} = \frac{Q_j - Q_i}{|\mathbf{x}_j - \mathbf{x}_i|}$.

After having rearranged the terms, the linearised version of (2.6) can then be written as

$$R_i^V = \frac{1}{V_i} \sum_{j \in E_i} BM^{-1} \frac{\partial Q}{\partial l} \triangle s_{ij},$$

where B is a 5×5 matrix calculated with respect to the primitive variables $\tilde{\mathcal{Q}} = (\rho, u, v, w, p)^T$, and M is the transformation matrix $M = \dfrac{\partial\mathcal{Q}}{\partial\tilde{\mathcal{Q}}}$.
The corresponding preconditioner is

$$\left(P_i^V\right)^{-1} = \frac{1}{V_i} \sum_{j \in E_i} BM^{-1} \frac{1}{|\mathbf{x}_j - \mathbf{x}_i|} \triangle s_{ij}. \tag{2.7}$$

Finally, the full matrix preconditioner is

$$P_i^{-1} = \left(P_i^I\right)^{-1} + \left(P_i^V\right)^{-1}. \tag{2.8}$$

3 Boundary Condition

To form the block-Jacobi preconditioner, the inviscid and viscous Jacobians need to be calculated at each node of the grid. However, at the wall, as already mentioned, the viscous Jacobian does not have to be evaluated. In fact, only a no-slip condition has to be satisfied which is achieved by setting all momentum components in the residual to zero. For Euler calculations, the procedure is slightly different. In addition to the corrections made on the residual, the preconditioner is modified at the wall in order that the condition $\mathbf{u}.\mathbf{n} = \mathbf{0}$ is satisfied; $\mathbf{u}$ and $\mathbf{n}$ denote respectively the velocity vector and the unit normal vector to the wall. This is accomplished by re-evaluating the matrix in the coordinate system (x_n, x_{t_1}, x_{t_2}), by using a rotation matrix T from the original (x, y, z) coordinate system to the new one. x_n is the coordinate in the direction normal to the surface and the other two are mutually orthogonal tangential coordinates. Once done, it is transformed back to the original coordinate system. Thus, equation (2.1) becomes

$$\left[P^{-1} - T^{-1}ST(P^{-1} - I)\right] \frac{dQ}{dt} = (I - T^{-1}ST)R, \tag{3.1}$$

where S is the matrix which sets the normal momentum component to zero. $T^{-1}ST$ only involves the unit normal vector.

4 Results

The results to be presented compare the use of matrix and scalar (local timestep) preconditioning. The inviscid calculations use full-coarsening V-cycle multigrid whereas the viscous calculations use semi-coarsening. The fine grid is collapsed twice to produce coarse grids for the multigrid sequence [5], and the iterative scheme used to converge the discrete residuals to zero is pseudo time-stepping using the 5-stage Runge-Kutta method developed by Martinelli [7], with CFL number equal to 2.5 on each mesh. The turbulence model is the one equation model developed by Spalart and Allmaras [15], and follows the same iterative scheme. The 5×5 block-Jacobi preconditioner is computed for each node before the first stage of each time step, then inverted and multiplied by the residual vector. To prevent singularities at stagnation points, the matrix preconditioner requires an entropy fix. Although the van Leer [16] entropy fix is used for the characteristic smoothing in the residual evaluation, the more severe Harten [6] treatment is used for the preconditioner with the minimum of the bounding parabola equals to one eighth the speed of the sound. All the calculations have been performed on a IBM SP2, using six nodes, except from the 3D viscous bypass duct problem, which has been performed on a SGI Power Challenge.

4.1 2D Viscous

Firstly, we consider the standard 2D RAE2822 airfoil test case 9 [9] ($M_\infty = 0.73$, $\alpha = 2.8$, $Re = 6.5 \times 10^6$). The calculations have been performed on a grid with 11298 nodes, with a maximum cell aspect ratio on the airfoil surface of 5238. The first point nearest to the wall is fixed such that at this point $y^+ < 1$. In Figure 1, we show the pressure contour plot, the skin friction and the convergence history. The computed pressure distributions compare well with the experimental data, and the shock is well captured, even if a bit forward of the experimental location, behaviour which has been previously observed [15].
Convergence of the Navier-Stokes residuals is shown for the new block-Jacobi preconditioner with semi coarsening strategy and the standard approach with scalar preconditioner. Both converge to machine accuracy, along with the turbulence model. The new approach yields computational savings of a factor 3. In term of asymptotic performance, the computational speedup is roughly a factor 10.
Figure 2 shows a bypass duct of a turbofan engine with the fine grid of the sequence used for the multigrid acceleration, the Mach contour plot and the convergence history for both approaches. The flow is from left to right, with periodic boundary conditions top and bottom. Here there is a row of struts and a pylon; the latter is treated with inviscid boundary conditions to reduce the computational requirements of the calculation, and because the purpose of studying this geometry did not require the pylon boundary layer to be resolved. The grid resolution used for each of the blades in the row is roughly equivalent to that used for the RAE2822 airfoil and the mesh has 55006 grid points. The Mach contours reveal that the turbulent wake emanating from the blade row disappears when the grid cannot resolve it. If the location of the wake was of paramount importance then grid adaption would be required. The oscillation which can be seen on the convergence history is present in both approaches. This is explained by the fact that the boundary layer is still not fully developed and during the transients there are some moving shocks and tiny separation bubbles at the leading edge of some of the struts. By comparing the two approaches when these phenomenoms have com-

pletely vanished, one can again identify a computational saving of approximately a factor 3.

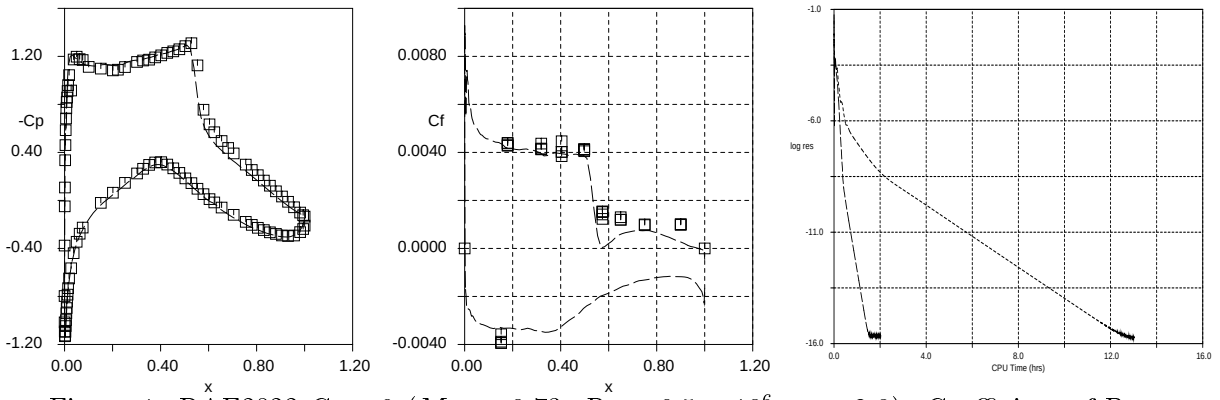

Figure 1: RAE2822 Case 9 ($M_\infty = 0.73$, $Re = 6.5 \times 10^6$, $\alpha = 2.8$). Coefficient of Pressure, Skin Friction, Convergence History.

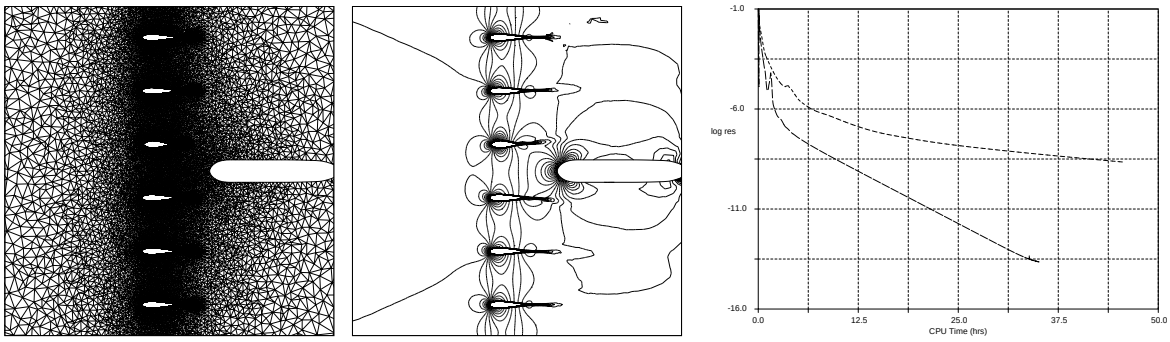

Figure 2: 2D Bypass duct geometry ($M_{inlet} = 0.55$, $Re = 10^6$, $\alpha = 0$). Fine grid, Mach contours and convergence history.

4.2 3D Inviscid

Here, we demonstrate the 3D inviscid capability of the method through the ONERA M6 wing test case. The grid considered has 124249 nodes with a maximum aspect ratio of 15, and the test case is $M_\infty = 0.84, \alpha = 3.06$. Comparison with experimental data [14] shows that the grid resolves properly the lambda shock structure, which is depicted in Figure 3. Looking at the convergence history, it appears that the gain due to the preconditioner is not as good as for the viscous cases. This lack of efficiency is explained by the grid which could be improved to be more regular with a smaller maximum aspect ratio, since some 2D investigations have demonstrated that a better grid with moderated stretched cells leads to computational savings comparable to [12], precisely between a factor three and four for asymptotic convergence. In addition, one must keep in mind that for such cases, the errors that are high frequency in one direction, but low frequency in the other direction, and which are well damped by a multigrid semi-coarsening strategy for viscous cases, are here not treated as efficiently. Thus, only a factor of 1.8 improvement is achieved for engineering accuracy.

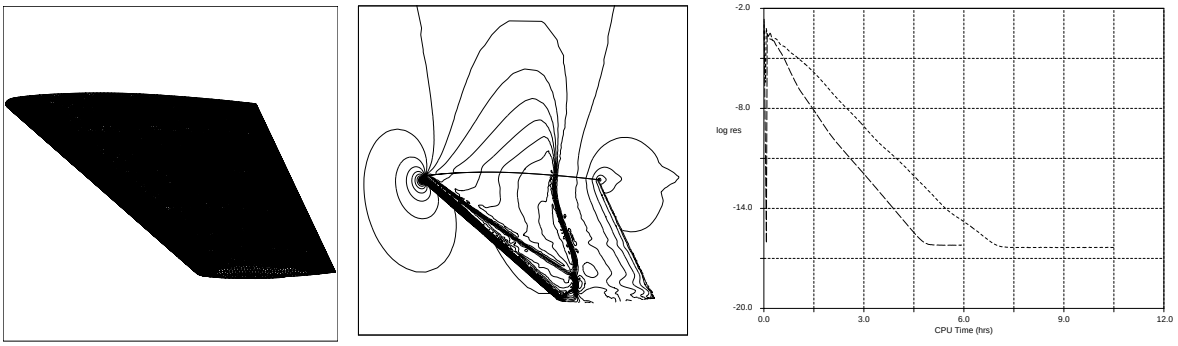

Figure 3: M6 wing ($M_\infty = 0.84$, $\alpha = 3.06$). Fine grid, Mach contours and convergence history.

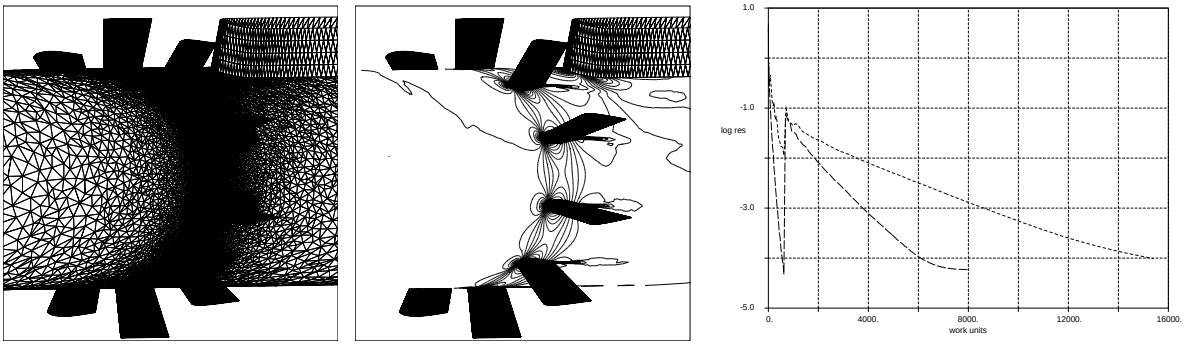

Figure 4: 3D Bypass duct geometry ($M_{inlet} = 0.55$, $Re = 10^6$, $\alpha = 0$). Fine grid, Mach contours and convergence history.

4.3 3D Viscous

The last example that we show is the 3D bypass duct problem. The grid has 274730 grid points and is constructed by stacking a sequence of 2D grids, and the one located at the tip (outer annulus) is exactly that used in Figure 2. Grid, Mach contours and convergence history can be seen in Figure 4. It is important to notice that the grid has high aspect ratios in the radial direction, which is a consequence of the grid being composed of stacked 2D grids with a fixed radial step, producing a high aspect ratio in the radial direction in all the regions of the 2D grid that have much smaller mesh spacing than the radial step and also across the boundary layer. Looking at the convergence history, where a work unit is a Runge Kutta step on the finest grid, one can already appreciate the benefits of the block-Jacobi preconditioner, almost a factor three. However, after three orders of magnitude, the residual does not reduce further. This needs some further investigation, but it is thought that this is due to the poor grid resolution, and a limit cycle associated with the limiters used in the higher-order residual discretisation.

5 Conclusion

An efficient preconditioned multigrid method has been implemented and tested for both inviscid and viscous flow applications. The standard scheme employing the usual scalar

preconditioner works quite well for Euler cases, but is less effective for turbulent Navier-Stokes calculations, due to stiffness introduced by the highly stretched cells in the boundary layer. The block-Jacobi preconditioner, in conjunction with a semi-coarsening multigrid strategy for the viscous cases, improves the damping of stiff modes. In all cases, the convergence rate is significantly enhanced, although some more investigation is needed for complex 3D geometries. In 2D, the improvement in convergence rate ranges from a factor 3 for engineering accuracy for inviscid and viscous cases to 4-10 for asymptotic convergence.

6 Acknowledgements

We wish to thank J. Elliott (MIT) for considerable advice on implementing the slip boundary condition adjustment to the preconditioner. The first author gratefully acknowledges the funding of the European Community.

References

[1] S. R. Allmaras. Analysis of a local matrix preconditioner for the 2-D Navier-Stokes equations. *AIAA 93-3330-CP*, 1993.

[2] P. I. Crumpton, M. B. Giles, and G. N. Shrinivas. Design optimisation for complex geometries. 15th ICNMFD Conference, Monterey, USA, June 1996.

[3] P.I. Crumpton and M.B. Giles. Aircraft computations using multigrid and an unstructured parallel library. AIAA Paper 95-0210, 1995.

[4] P.I. Crumpton and M.B. Giles. Implicit time accurate solutions on unstructured dynamic grids. *International Journal for Numerical Methods in Fluids*, 25:1285–1300, 1997.

[5] P.I. Crumpton, P. Moinier, and M.B. Giles. An Unstructured Algorithm for High Reynolds Number Flows on Highly-Stretched Grids. In C. Taylor and J. T. Cross, editors, *Numerical Methods in Laminar and Turbulent Flow*, pages 561–572. Pineridge Press, 1997.

[6] A. Harten. High resolution schemes for conservation laws. *Journal of Computational Physics*, 49:357–393, 1983.

[7] L. Martinelli. *Calculations of Viscous Flows with a multigrid method.* PhD thesis, Dept. of Mech. and Aerospace Eng., Princeton University, 1987.

[8] D. Mavriplis. Three-dimensional multigrid for the Euler equations. *AIAA Journal*, 30(7):1753–1761, July 1992.

[9] P. Cook M. McDonald and M. Firmin. Airfoil RAE 2822 - Pressure distributions, and boundary layer wake measurements. *AGARD AR-138*, page A6, 1979.

[10] W.A. Mulder. A new multigrid approach to convection problems. *Journal of Computational Physics*, 83:303–323, 1989.

[11] J. Peraire J. Peiró and K. Morgan. A 3D finite-element multigrid solver for the Euler equations. *AIAA Paper 92-0449*, January 1992.

[12] N. A. Pierce and M. B. Giles. Preconditioned multigrid methods for compressible flow calculations on stretched meshes. *J. of Computational Physics*, 136:425–445, 1997.

[13] N.A. Pierce and M.B. Giles. Preconditioning compressible flow calculations on stretched meshes. AIAA Paper 96-0889, 1996.

[14] V. Schmidt and F. Charpin. Pressure distributions on the M6 wing at transonic Mach number. AGARD, 138, 1979.

[15] P. R. Spalart and S. R. Allmaras. A one-equation turbulence model for aerodynamic flows. *La Recherche Aérospatiale*, 1:5–21, 1994.

[16] B. van Leer, W-T. Lee, and K.G. Powell. Sonic–point capturing. AIAA Paper 89-45-CP, The University of Michigan, Department of Aerospace Engineering, 1989.